Mechanogenetic Coupling of *Hydra* Symmetry Breaking and Driven Turing Instability Model

Jordi Soriano,[‖†] Sten Rüdiger,[‡*] Pramod Pullarkat,[§] and Albrecht Ott[¶]
[†]Department of Physics of Complex Systems, Weizmann Institute of Science, Rehovot, Israel; [‡]Institut für Physik, Humboldt-Universität zu Berlin, Berlin, Germany; [§]Raman Research Institute, Bangalore, India; [¶]Experimentalphysik, Universität des Saarlandes, Saarbrücken, Germany; and [‖]Dept. ECM, Facultat de Física, Universitat de Barcelona, Barcelona, Spain

ABSTRACT The freshwater polyp *Hydra* can regenerate from tissue fragments or random cell aggregates. We show that the axis-defining step ("symmetry breaking") of regeneration requires mechanical inflation-collapse oscillations of the initial cell ball. We present experimental evidence that axis definition is retarded if these oscillations are slowed down mechanically. When biochemical signaling related to axis formation is perturbed, the oscillation phase is extended and axis formation is retarded as well. We suggest that mechanical oscillations play a triggering role in axis definition. We extend earlier reaction-diffusion models for *Hydra* regrowth by coupling morphogen transport to mechanical stress caused by the oscillations. The modified reaction-diffusion model reproduces well two important experimental observations: 1), the existence of an optimum size for regeneration, and 2), the dependence of the symmetry breaking time on the properties of the mechanical oscillations.

INTRODUCTION

Spontaneous symmetry breaking is a well studied aspect of self-organization and pattern formation. There are numerous examples of spontaneous symmetry breaking in physics, among them equilibrium phase transitions or out-of-equilibrium systems that develop macroscopic spatial gradients. Spontaneous symmetry breaking may also appear as a crucial step during biological development. Although development builds on an initial asymmetry for embryonic axis definition in higher animals and plants (e.g., initial molecular inhomogeneities in *Drosophila* (1) or the sperm entry point in the *Xenopus* egg (2)), ancient multicellular organisms could use spontaneous symmetry breaking as a strategy for axis definition. A well studied case is the zygote of the brown algae *Fucus* (3). The zygote is initially symmetric and defines its polarity after the first cell division. The absence of initial asymmetries before axis definition is revealed by the possibility of orienting and reorienting the polarity of the zygote by a number of environmental gradients, such as light or gravity.

Here, we study spontaneous symmetry breaking mechanisms during the regeneration of the freshwater polyp *Hydra vulgaris*. This 1-cm-long animal consists of a cylindrical body column with a mouth surrounded by tentacles at one end and a foot at the other. The body column is made of a bilayer of omnipotent cells that are in a continuous state of proliferation. Cells that originate in the body column migrate to the extremities, where they differentiate irreversibly and form specialized tissues before they die.

Hydra development is controlled by a small group of cells located at the apical part of the head, a region called the hypostome. This group of cells constitutes an organizing center known as the ''head organizer'' (4–7). Signals generated in this region are transmitted to the body column to set up a gradient of positional information that organizes and patterns the animal (7–9). A number of signaling molecules have been identified in *Hydra* patterning (10). Among them, the Wnt signaling pathway plays a pivotal role in axis formation (4,6).

The continuous state of growth, tissue differentiation, and replacement in *Hydra* is the basis for its astonishing regeneration capabilities (7,11,12). Gierer et al. (13), and later others (14,15), showed that positional information is destroyed in an aggregate of dissociated *Hydra* cells and de novo symmetry breaking is required. The aggregate is able to regenerate in 2–3 days at room temperature. Only one animal forms for small aggregates, and typically more than one animal emerges if the initial aggregate contains a large number of cells (15).

Positional information is lost as well in sufficiently small fragments cut out of *Hydra* tissue (16,17). Despite the fact that in tissue fragments the cells are not randomized in their relative position, they subsequently develop just like initially isotropic aggregates. Hence, the developing structure from small fragments needs to perform symmetry breaking in a manner indistinguishable from that of aggregates (17).

In its regeneration, *Hydra* first forms an elastic hollow cell ball made of a cell bilayer that displays repeated cycles of inflation and rapid collapse upon rupture. The mechanical aspects of *Hydra* patterning were initially studied by Beloussov et al. (18), and the inflation-collapse cycles were subsequently explored by others (16,19). The spherical symmetry is broken at a later stage of development, when *Hydra* creates a weak spot in the cell ball, which reduces the inflation amplitude (17). As a result of the symmetry breaking process, the regenerating *Hydra* develops a group of irreversibly differentiated cells that constitute the head organizer. This is the first structure to be formed or restored during regeneration (12). The organizer controls subsequent

Submitted April 1, 2008, and accepted for publication September 24, 2008.

*Correspondence: sten.ruediger@physik.hu-berlin.de

Editor: Herbert Levine.

0006-3495/09/02/1649/12 $2.00

doi: 10.1016/j.bpj.2008.09.062

development, and regeneration is completed with the formation of head, tentacles, and foot.

The regeneration capabilities of *Hydra* and its patterning process have given rise to models for biological pattern formation. In a pivotal work, Turing showed how a two-species chemical reaction with large contrasts in species lifetimes or diffusion coefficients results in a pattern-forming instability (20). Turing was also the first to recognize the possible significance of reaction-diffusion (RD) processes for *Hydra* development. He discussed, in particular, the regrowth of tentacles from a circular ring at the head end. Today, RD equations are often used to describe pattern formation in biology (21). Turing reactions have already been identified and mapped to molecular components in bone growth (22), and recently, molecular evidence for an activator-inhibitor mechanism has been found in the development of embryonic feather branching (23).

Particularly since the work of Meinhardt and co-workers (24–26), RD equations have been used extensively to describe the regrowth of *Hydra*, for instance, after loss of body parts such as the foot or head. Although in *Hydra*, activator and inhibitor molecules or ''morphogens'' have not yet been identified, such models can claim to reproduce nearly all of the typical features of regrowth. They may be considered as a useful reduction of the system's complexity, with a certain predictive power.

Here, we present experimental evidence that the inflation-collapse cycles are an indispensable component of *Hydra* symmetry breaking, and that the chemical RD picture needs to be extended by means of biomechanical coupling. We propose that mechanical stress, driven by the oscillations, creates the biochemical conditions for the system to undergo a Turing instability and to develop a pattern.

Our experimental results and their analysis in the framework of an extended RD model provide, to our knowledge, the first conclusive evidence that mechanical stimulation plays a fundamental role in *Hydra* development. It is interesting to note that a connection between gene expression and mechanical stimulation has been revealed in detail in *Drosophila* patterning (27,28) and in the formation of capillary blood vessels (29).

METHODS

Hydra culturing

Experiments were carried out with strains of *Hydra vulgaris*, provided by T. C. G. Bosch (University of Kiel, Kiel, Germany). The animals were cultured at 18°C in *Hydra* medium (1.0 mM $CaCl_2$, 1.5 mM $NaHCO_3$, 0.1 mM $MgCl_2$, 0.08 mM $MgSO_4$, and 0.03 mM KNO_3), fed regularly four times a week, and starved for 24 h before manipulation for experiments.

Hydra spheres preparation

Hydra spheres were obtained either from small fragments of tissue or from aggregates of dissociated single cells. The different preparations that we studied are summarized in Fig. 1 *A* and Table 1. Spheres derived from small tissue fragments were prepared as described in two previous studies (16,17). Briefly, preparation consisted of cutting a thin disc of tissue from the central part of the body column of an adult *Hydra*. The disc was divided into four to eight fragments of different sizes, and left for 2 h at 20°C. The fragments closed and healed at the edges, forming hollow spheres made of a cell bilayer with initial radii typically between 100 and 170 μm. The minimum radius of spheres that successfully regenerated was 100 μm.

Hydra balls derived from large tissue fragments were also prepared to study radii >170 μm. These spheres were obtained using the same procedure described above, but without splitting the disc of tissue into smaller fragments, or by directly cutting arbitrarily large fragments of tissue.

We also studied small spheres derived from buds formed during the asexual reproduction of *Hydra*. Buds were excised at early stages of development, when they started to emerge from the body column of the adult

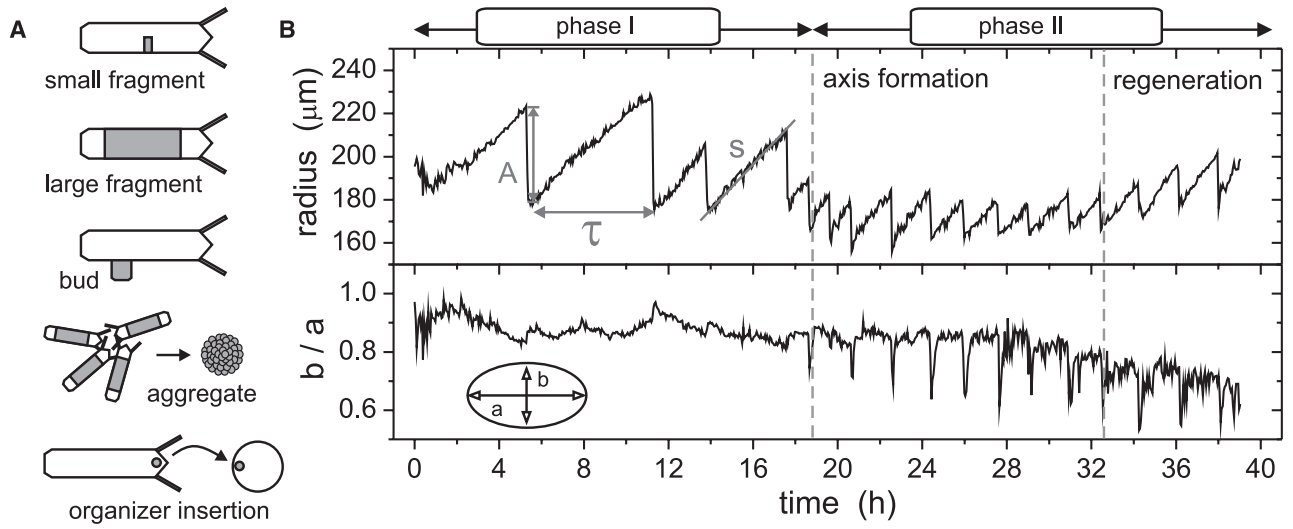

FIGURE 1 (*A*) Sketch of the different *Hydra* sphere preparations and tissue manipulations (see Methods for details). (*B*) Mechanical oscillations during regeneration of a small fragment of *Hydra* tissue, showing the evolution of the average radius of the sphere and the ratio between the minor and major axes as a function of time. Phase I and phase II denote the stages of isotropic and anisotropic motion, respectively.

TABLE 1 Summary of the different tissue manipulations used to prepare *Hydra* spheres, typical range of sizes, and mechanical behavior during regeneration

Preparation	r_0 (μm)	Initial polarity	Phases
Small fragments	100–200	No	I + II
Large fragments	$\geq$250	Yes	II
Buds	100–200	Yes	II
Aggregates	150–1500	No	I + II
Organizer incorporation	100–200	No (induced)	I (short) + II

Hydra. Excised buds were left for 2 h to form hollow spheres with radii in the range 100–200 μm.

Spheres derived from aggregates of dissociated single cells were prepared as follows. After removal of the head and foot, a group of 3–10 adult animals was cut into small fragments, which were treated with dissociation medium (3.6 mM KCl, 6 mM $CaCl_2$, 1.2 mM $MgSO_4$, 6 mM sodium citrate, 6 mM sodium pyruvate, 6 mM glucose, 12.5 mM TES, and 50 mg/ml rifampicin, pH 6.9) for 2–4 h at 4°C. During this time, fragments underwent repeated pipetting of the suspension, periodic cycles of filtering, centrifugation, and resuspension in fresh dissociation medium to improve the dissociation. A compact aggregate of cells was obtained by centrifugation of the final solution for 10 min at 10 $\times$ *g*. The aggregate was left to stabilize in 50% dissociation medium/50% *Hydra* medium for 2 h at 20°C, and finally transferred to 100% *Hydra* medium. A hollow sphere emerged from the aggregate of cells within 4–6 h. Different sphere sizes were obtained by splitting the cell suspension into populations of different sizes before the final centrifugation step. The final sizes obtained varied between 150 and 1500 μm in radius.

Staurosporine-treated *Hydra* spheres

We followed the experimental procedure described by Cardenas et al. (30). Staurosporine was obtained from Sigma (St. Louis, MO), and we used ethanol as the solvent. Spheres were cultured at 20°C in the presence of inhibition medium consisting of 1 μM staurosporine solution in *Hydra* medium. We immersed control spheres in inhibition medium without staurosporine to verify that the solvent was not toxic for the animals.

Incorporation of preactivated cells into *Hydra* spheres

To incorporate preactivated cells into the prepared *Hydra* spheres, we followed the experimental procedure described by Technau et al. (15). An adult *Hydra* was beheaded and left unperturbed for 12 h to constitute a new head organizer. Next, a small, 20- to 50-cell region of the apical end of the regenerating animal was excised. This cell community was then stained by immersing it for 1 min in a solution that contained one part 1,1′-dioctadecyl-3,3,3′,3′-tetramethylindocarbocyanine perchlorate (Dil) and nine parts 70-mM sucrose solution in *Hydra* medium, using the procedure implemented by Kishimoto et al. (31). The stained cells were finally inserted into a newly created *Hydra* cell ball. The *Hydra* sphere was left unperturbed to regenerate normally, and its evolution was monitored as described below. Periodic snapshots of the *Hydra* ball under fluorescent light were acquired to trace the location of the stained cells.

Monitoring the evolution of *Hydra* spheres

The spheres were transferred immediately after preparation into a recording chamber consisting of a petri dish 30 mm in diameter filled with *Hydra* medium. The chamber contained a series of 10 wells made of solidified agarose gel with a diameter of 1 mm and a separation distance of 1 mm. Each well contained a single *Hydra* sphere. The spheres quickly stuck to the surface of the chamber, which prevented them from moving or rotating. The chamber was mounted on the *xy* stage of a home-built microscope equipped with a 5X Zeiss Epifluar objective. Using a CCD camera to follow the evolution of the *Hydra* spheres, images 574 $\times$ 512 pixels in size were recorded at 3-min intervals over 2–4 days or until regeneration was completed. A computer controlled the acquisition of the images, which were synchronized with the movement of the *xy* stage. The spheres were kept in darkness and illuminated only during image acquisition. Those spheres that had not completed regeneration by the end of the experiment were excluded from further analysis. All experiments were carried out at 20°C.

Data analysis

Images were analyzed to retrieve the in-plane contour of the *Hydra* ball as a function of time. The mechanical changes of the *Hydra* ball during regeneration were described in terms of the radius, r, defined as $r = (S/\pi)^{1/2}$, where S is the area enclosed by the contour of the sphere. Since *Hydra* balls evolved from a sphere to an ellipsoid during regeneration, the changes in the *Hydra* shape were quantified by fitting the contours to an ellipse and extracting the major axis, a, and the minor axis, b. Local variations in the shape of the evolving *Hydra* were obtained by comparing the relative variation of contours at different times.

Hydra spheres show periodic inflation-collapse cycles during regeneration. To systematically compare different *Hydra* spheres, each $r(t)$ plot was analyzed to extract, for each cycle, the minimum and maximum radii, r_{min} and r_{max}, the time interval between two cycles, τ, and the swelling rate, dr/dt, which was obtained as a linear fit during the inflation stage (Fig. 1 *B*). From these quantities we obtained the amplitude of the oscillations, $A = \langle r_{max} - r_{min} \rangle$, the frequency of the oscillations $f = 1/\langle \tau \rangle$, and the average swelling rate, $s = \langle dr/dt \rangle$, where $\langle \ldots \rangle$ indicates the average over cycles. We also defined the characteristic radius of the sphere as $r_0 = \langle r_{min} \rangle$, which allows us to systematically compare spheres of different sizes and from different preparation techniques.

Hydra spheres with higher outer osmolarity

We used the method described in Kücken et al. (19) to study the regeneration process of *Hydra* spheres with higher osmotic concentrations outside the *Hydra* shell. Only spheres derived from small fragments of tissue were used in these experiments, and they were prepared as follows. Immediately after cutting, fragments were immersed in a chamber containing *Hydra* medium and were left for 2 h so that the fragments trapped the medium inside the *Hydra* ball during closure and formation of the sphere. The spheres were next transferred to the final recording chamber containing the final medium at the outer concentration C_{out}, and their evolution was monitored as described above. We always used *Hydra* medium as inner concentration C_{in}, and as standard procedure (19,32), outer concentrations with increased osmolarity were obtained by adding sucrose to *Hydra* medium. The sucrose concentration differences, $\Delta C = C_{out} - C_{in}$, that we studied varied between 0 and 100 mM, in steps of 12.5–25 mM. Control experiments with adult *Hydra* were carried out to verify that the concentrations were not toxic for the animals.

Phosphorylation assay

Hydra spheres (~300) derived from small fragments of tissue were prepared according to the standard procedure and cultured in darkness at 20°C for a precise time, between 4 and 60 h, in steps of 3–12 h, to study different regeneration stages. The spheres were quickly analyzed at the end of each preset culture time to obtain the distribution of sizes and a quantification of the total number of cells. Next, the proteins from the *Hydra* spheres were extracted with 200 μl phosphate-buffered saline (PBS) + 1% TritonX, 20 μl aprotinin, and 20 μl leupiptin. Three consecutive cycles of freezing (liquid nitrogen, 3 min) and unfreezing (water bath at 37°C, 2 min) were then applied, and PBS + 1% TritonX was added to achieve a final volume of 400 μl. The solution was dialyzed for ~24 h at 4°C with PBS. A 50-μl amount of the dialyzed protein was taken for the enzyme-linked immunosorbent assay (ELISA) analysis. Wells in a Maxisorp plate (Nunc, Rochester, NY) were coated with 6 μg/ml of anti-HZO-1 (Sigma) in 50 μl coating buffer (0.1 M carbonat/bicarbonate buffer, pH 9.6) overnight at 4°C. The

wells were then washed three times with 200 μl PBST, and blocked with 200 μl blocking buffer (1% BSA, 1% FBS in PBS) for 2 h at room temperature. Next, 50 μl of the dialyzed protein were placed into the wells, and incubated at 37°C for 2 h in a wet chamber. Plates were washed three times with 200 μl 0.05% Tween in PBS (PBST), and 50 μl of antiphosphotyrosine 1:5000 (Biosource, Camarillo, CA) in blocking buffer were added to each well, and incubated again at 37°C for 1 h in a wet chamber. Plates were washed three times with 200 μl PBST, and 50 μl anti-mouse HRPOD 1:2000 (Dianova, Hamburg, Germany) in blocking buffer was added to each well. After 1 h of incubation at room temperature, plates were washed three times with 200 μl PBST, and developed with 200 μl TMB (Sigma) for 15 min. The reaction was stopped with 100 μl 0.5 M H_2SO_4. The concentration was measured in an ELISA reader at 450 nm. The concentration measured was finally rescaled with the number of cells.

EXPERIMENTAL RESULTS

Mechanical oscillations and shape change in regenerating *Hydra* spheres

Regenerating *Hydra* form hollow spheres that, after closure, exhibit characteristic inflation-collapse cycles of steady swelling, rupture, and collapse (Fig. 1 *B*) (16,17). In a first stage (phase I), the cycles are of large amplitude and low frequency, and the *Hydra* ball maintains a spherical shape. This isotropic motion is revealed by analysis of the ratio between the minor axis, b, and the major axis, a, of the *Hydra* contour, which is practically constant (Fig. 1 *B*). In a second stage (phase II), the cycles change to a new scenario of small amplitude and high frequency. The shape of the *Hydra* ball changes to an ellipsoid, with a corresponding to the future foot-head axis of the animal. The ratio between the minor and major axis peaks toward 0 during deflation (Fig. 1 *B*), revealing anisotropic elasticity and motion.

The transition from phase I to phase II identifies the symmetry breaking moment, t_{SB}, and signals the formation of the new axis (17). Once the axis is established, regeneration completes in 1-2 days.

The two-phase motion is observed for small fragments of tissue, with radii $r_0 \lesssim 200$ μm. It is also characteristic of aggregates of any size. Large fragments or spheres derived from excised buds show phase II motion only (17).

Table 1 summarizes the behavior of *Hydra* spheres obtained from different tissue manipulations. We conclude that the presence of phase I motion identifies mechanically isotropic spheres, and that spheres with only phase II (large fragments and buds) retain anisotropy from the original tissue and do not require symmetry breaking. Large fragments maintain the axis and keep the foot-head polarity of the original tissue. Buds, on the other hand, have an organizer already formed (4), and therefore, both axis and foot-head polarity are already defined.

Dependence of symmetry breaking time on sphere size, swelling rate, and frequency

To assess the relation between symmetry breaking and the parameters of the oscillating sphere, we have investigated the behavior of ~100 isotropic spheres derived from fragments with radii, r_0, in the range 100–200 μm. In this section, we describe the dependence of the symmetry breaking time, t_{SB}, on sphere size, r_0, swelling rate, s, and frequency of oscillations, f.

The dependence of t_{SB} on r_0 is shown in Fig. 2. The symmetry breaking time decreases with size up to a radius of ~140 μm, to increase again for spheres of larger radius. The behavior is well described by a parabolic fit, and suggests that there is an optimal radius, $r_c \simeq 138$ μm, that minimizes the time required for symmetry breaking.

To characterize the dependence of t_{SB} on the swelling rate, s, and on the frequency of oscillations, f, we carried out experiments with spheres of similar radius, $r_0 \simeq 150$ μm, and we gradually increased the concentration difference, ΔC, between the inner medium, C_{in} (*Hydra* medium), and the outer medium, C_{out} (sucrose in *Hydra* medium). We studied sucrose concentrations in the range 0–100 mM in steps of 12.5–25 mM. As shown in Fig. 3 *A*, the effect of increasing ΔC is to reduce the swelling rate, s, and increase the cycle duration, τ (reduce f). The swelling rate, s, decreases almost linearly with ΔC until, at $\Delta C \geq 100$, no swelling is observed (Fig. 3 *B*).

The effect of a gradually higher ΔC on symmetry breaking is shown in Fig. 3 *C*. The symmetry breaking time, t_{SB}, increases with ΔC. For $\Delta C \geq 100$ mM, which also corresponds to a swelling rate $s \simeq 0$, symmetry breaking does not occur and the spheres do not regenerate.

We have observed that the time span between symmetry breaking and regeneration is insensitive to ΔC. Hence, those spheres that break the symmetry also regenerate normally,

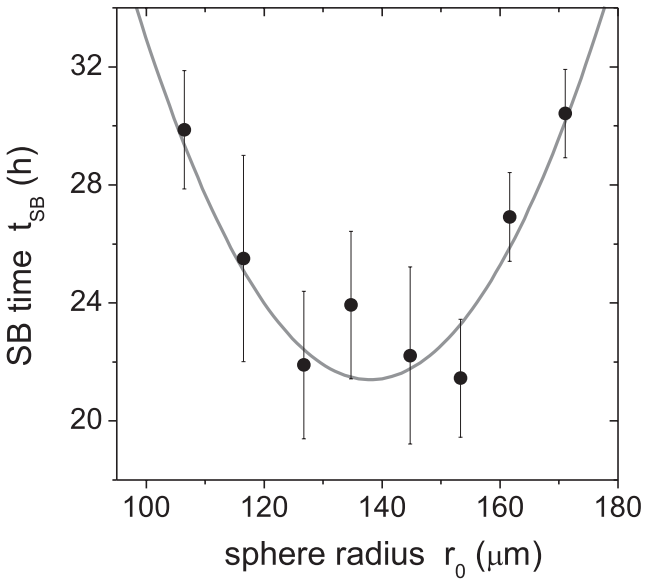

FIGURE 2 Dependence of the symmetry breaking time, t_{SB}, on the size of the sphere, r_0. Each point is an average over 7–15 spheres of similar size. The curve is a parabolic fit of the form $t_{SB} = t_{min} + 152.3\ [(r_0/r_c - 1]^2$, with $t_{min} \simeq 21.4$ h and $r_c \simeq 138$ μm.

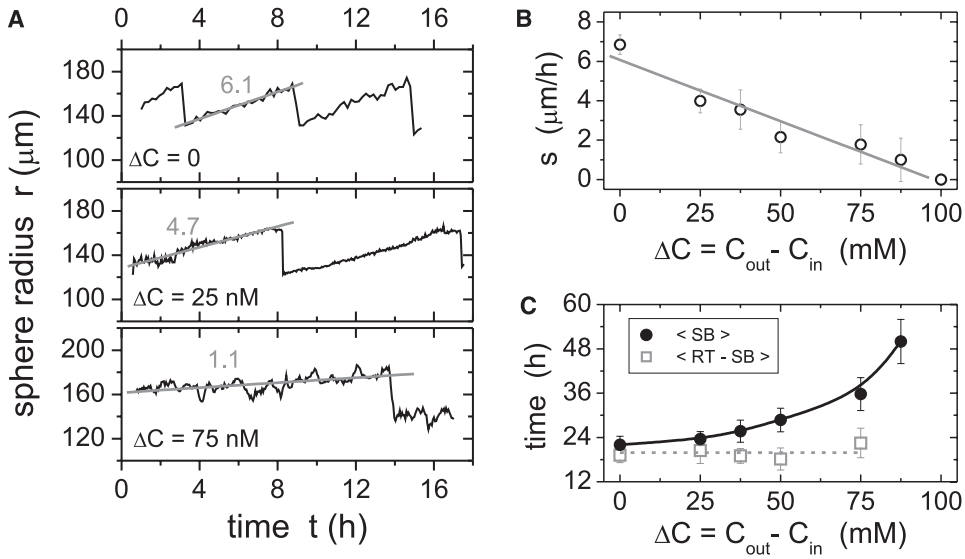

FIGURE 3 (*A*) Examples of inflation-contraction cycles for gradually higher osmotic concentration, $\Delta C = C_{out} - C_{in}$, with C_{in} *Hydra* medium and C_{out} sucrose in *Hydra* medium. The swelling rate dr/dt is obtained as linear fits during the inflation stage. (*B*) The average swelling rate, s, decreases linearly with ΔC, and at $\Delta C \geq 100$ mM, $s \simeq 0$. Each point is an average over two to five cycles per sphere, and over six spheres. (*C*) For the same spheres, the corresponding symmetry breaking time (*black dots*) increases with the concentration difference, ΔC, whereas the time difference between symmetry breaking and regeneration (*gray squares*) is insensitive to ΔC.

indicating that the presence of sucrose does not affect the metabolism of the animals. This has been also verified for large fragments, i.e., anisotropic spheres that lack phase I oscillations. We observed that they regenerate normally in the hyperosmotic medium.

Since the effect of ΔC is to decrease both the swelling rate, s, and the frequency of oscillations, f, we can characterize the variation of the symmetry breaking time in terms of these quantities. As shown in Fig. 4, *A* and *B*, t_{SB} rapidly decreases with s and f, according to a dependence that is well described by a function of the form $a/[(bx)^{\gamma} - 1]$, with x either s or f. The fits have been performed with a fixed exponent, $\gamma = 0.3$. This value arises from microrheological properties of cells (33) and will be discussed in the section on the RD model.

We conclude that isotropic spheres require the presence of oscillations to break the symmetry. The dependence of t_{SB} on s is a strong indication that axis formation is coupled to mechanical changes. To establish this direct link we take into account that the difference between regeneration time and symmetry breaking is insensitive to the osmotic difference, ΔC. Therefore, genetic changes appear not to be directly connected to sucrose levels, but may nevertheless be linked to them by the variation in swelling rate. Further evidence comes from the fact that at a constant sucrose level we still observe

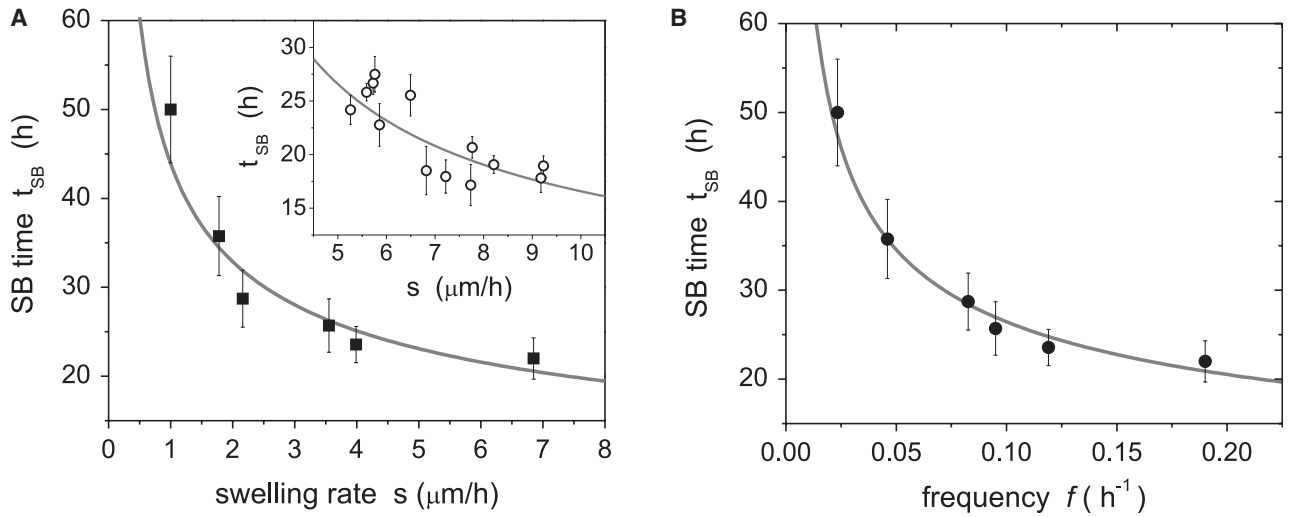

FIGURE 4 Dependence of the symmetry breaking time, t_{SB}, on the swelling rate, s, and the frequency of oscillations, f. (*A*) Main plot. The variation of t_{SB} as a function of s for *Hydra* spheres with different osmotic concentrations, ΔC, is well described by a fit of the form $a/[(bs)^{\gamma} - 1]$ (*gray curve*), where $a \simeq 97\ h$, $b \simeq 49\ h\ \mu m^{-1}$, and $\gamma = 0.3$. Each point is an average over two to five cycles per sphere, and over six spheres. (*Inset*) A similar scaling with the same exponent, γ, is obtained for a set of *Hydra* spheres with fixed $\Delta C = 0$ and size $r_0 \simeq 150\ \mu m$. Each point is an average over two to five cycles of the same sphere. (*B*) The variation of t_{SB} as a function of f for different ΔC also follows the dependence $a/[(bf)^{\gamma} - 1]$, with $a \simeq 106\ h$, $b \simeq 2142\ h$, and $\gamma = 0.3$. Each point is an average over two to five cycles per sphere, and over six spheres.

a clear dependence of t_{SB} on s (Fig. 4 *A*, *inset*). Note that for a fixed sucrose concentration, a range of s-values can be assessed due to the stochastic variation of s, i.e., each individual sphere has a slightly different swelling rate.

The similar scaling of t_{SB} with s and f suggests that the quantities s and f are linearly related. Indeed, this linearity can be understood, since the amplitude of the oscillations, A, remains about constant (at ~40 μm) for the entire range of ΔC (Fig. 3 *A*). Therefore, the factor A in the relation $Af = s$ is independent of ΔC and makes f and s proportional.

Cell differentiation after symmetry breaking

Regenerating *Hydra* spheres form a new axis at the symmetry breaking moment, an event that is correlated with the formation of the head organizer (17). The organizer irreversibly locks the axis and controls the patterning of the animal through the establishment of a new positional gradient.

A number of observations suggest that the changes induced by the organizer are translated into the tissue, i.e., at a cellular level. First, we have observed that deflation always occurs at a reduced amplitude during phase II compared to phase I (Fig. 1 *B*). Before symmetry breaking, the rupture point of the cell ball in each cycle occurs at different locations over the surface of the sphere. After symmetry breaking, however, rupture always occurs in the same place, the position of the future head, and corresponds to a permanent weak spot that functions as an early mouth (17). Following Hobmayer et al. (4), the emergence of a weak spot is associated with the expression of β-catenin and Wnt, and thus suggests the presence of a morphogen gradient in the regenerating *Hydra*. We therefore conclude that the beginning of phase II motion is correlated with the establishment of a biochemical pattern.

Second, the swelling rate of the *Hydra* ball significantly increases after symmetry breaking. As shown in Fig. 5 *A*, the distribution of swelling rates during phase I, obtained from the analysis of 30 spheres, has a narrow distribution with a mean of $\simeq 7.2$ μm/h. After symmetry breaking, the same spheres show a wider distribution of swelling rates, with a mean at $\simeq 10.5$ μm/h, a 45% increase. Since the swelling rate, as well as the shape, depends on the elasticity of the *Hydra* ball, this increase suggests that some regions of the sphere have permanently changed the elasticity and offer lower resistance to swelling.

And third, we note that at symmetry breaking, the *Hydra* ball irreversibly modifies its shape (from sphere to ellipsoid) and motion (isotropic to anisotropic). For the cases in which *Hydra* exactly regenerates parallel to the plane of observation, it is possible to study local changes in the shape of the animal by comparing consecutive contours. As shown in Fig. 5 *A*, the contour displays isotropic inflation and collapse before symmetry breaking, with all regions of the *Hydra* sphere inflating or deflating at practically the same rate (Fig. 5 *A*, *upper*). The isotropic motion disappears after symmetry breaking to become more complex. The poles of the *Hydra* ellipsoid deflate in opposite phase compared to the rest of the body (Fig. 5 *A*, *lower*). At later stages, when regeneration is almost completed and the *Hydra* shape has evolved to a cylinder, swelling and contraction is more active at the extremes of the cylinder than at the rest of the body. *Hydra* maintains an ellipsoidal or cylindrical shape after regeneration, and never recovers a spherical configuration unless it is cut again or the cells dissociated.

To establish a connection between these permanent shape modifications and changes at a cellular level, we have investigated phosphorylation in the tight junction, a protein scaffold part of the adhesion complex that is known to control volume and ion exchange in the paracellular space of epithelial cells. HZO-1 is the *Hydra* analog of the zona occludens protein, one of the tight junction constituents (34). As shown in Fig. 5 *B*, an ELISA of ~300 spheres at different regeneration stages reveals a substantial increase in phosphorylation of HZO-1 at symmetry breaking. In general, phosphorylation is known to play an important role during regeneration in *Hydra* and has been investigated in detail in recent years (see, e.g., (35,36)).

Phosphorylation data in Fig. 5 *B* is shown together with the change in the period of the inflation-collapse cycles, and reveals that the beginning of phase II motion indeed coincides with the increase in phosphorylation. Since the emergence of phase II is correlated with the formation of the organizer (17), we conclude that the organizer induces these biochemical changes at a cellular level.

On the other hand, staurosporine modifies phosphorylation signaling (37) and retards head differentiation in *Hydra* (30). To verify whether phase I motion is prolonged accordingly, we carried out experiments with staurosporine-treated spheres. As shown in Fig. 5 *C*, treated spheres significantly extend phase I, corroborating the connection between phosphorylation and organizer formation. Conversely, like Technau et al. (15), we observed that phase I can be shortened if a small cluster of cells from the apical end of a regenerating *Hydra* is inserted into a newly created *Hydra* sphere (Fig. 5 *C*). The cluster of preactivated cells acts as an organizer. It defines the polarity of the *Hydra* ball, with the region of incorporation corresponding to the future head of the animal.

The changes at a cellular level are strong, so that the removal of the organizer does not destroy the positional information. Large fragments are the most prominent example. They keep their elongated shape, lack symmetry breaking, and regenerate the missing parts (foot and head) with the original polarity. We obtained additional evidence with experiments in which we cut the poles of the regenerating *Hydra* sphere just after symmetry breaking (data not shown). Since the sphere evolves to an ellipsoid, it is possible to identify the axis, and by cutting the poles, we eliminate the new organizer. The animal neither recovers its spherical shape nor initiates symmetry breaking again.

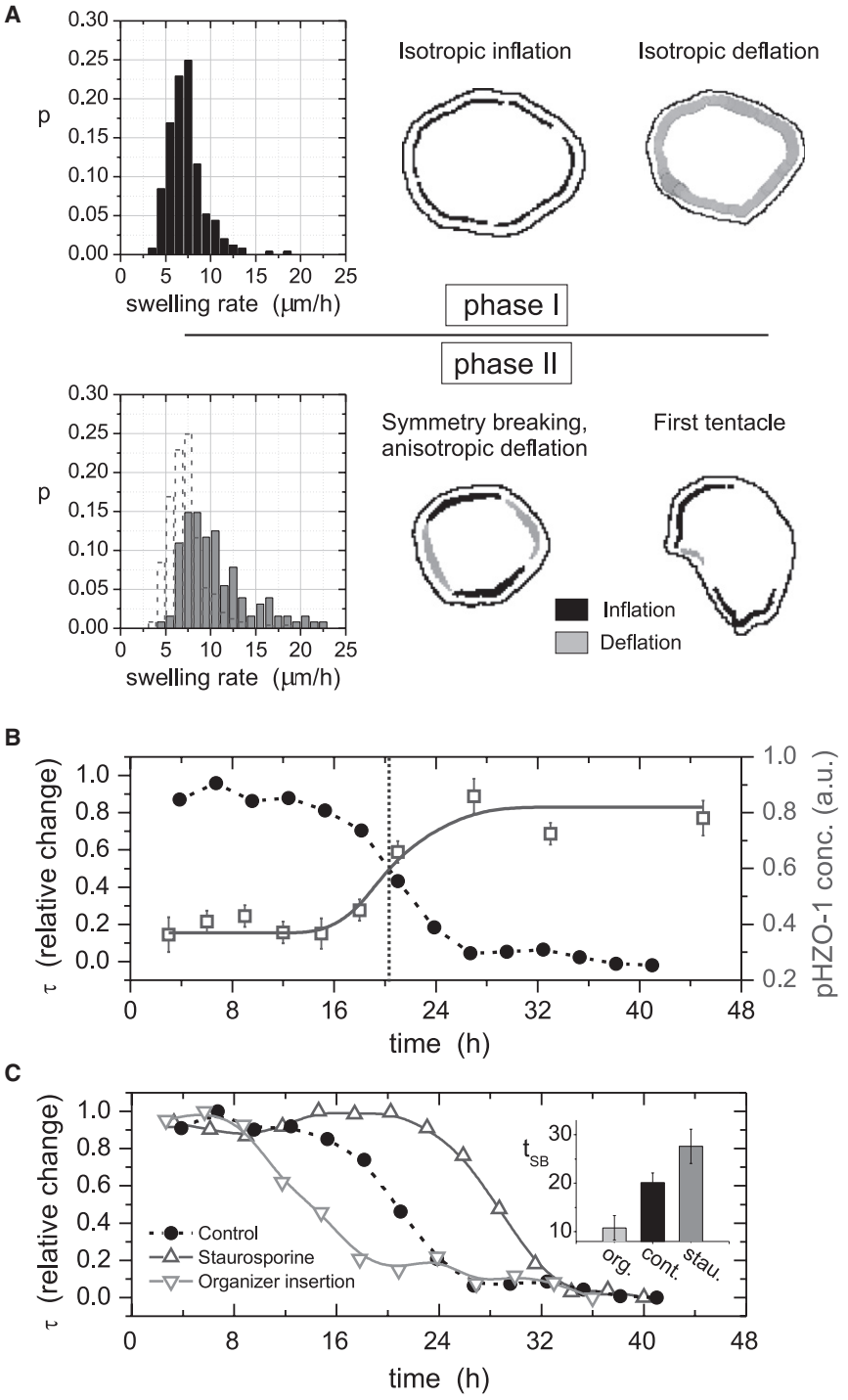

FIGURE 5 (*A*) Distribution of swelling rates and the relative change between consecutive contours during phase I (*upper*) and phase II (*lower*). The swelling statistics are obtained from 30 spheres of similar size, in the range $r_0 = 130$–150 μm, with a total of 150 cycles during phase I and 130 cycles during phase II. For the relative change between two consecutive contours, black and gray indicate inflation and deflation, respectively. The thickness of the color band is proportional to the variation between contours. (*B*) Time evolution of the amount of HZO-1 phosphorylation (*squares*) compared to the relative change of the period of the oscillations, τ, for spheres with $r_0 \simeq 150$ μm (*circles*, average over 20 experiments). The vertical line indicates the average symmetry breaking time. (*C*) Relative change in the period of the oscillations for spheres with $r_0 \simeq 150$ μm, and with staurosporine treatment (*up triangles*, average over three experiments), organizer incorporation (*down triangles*, six experiments), and control (*black*, 20 experiments). Lines are a guide to the eye. The inset shows the average symmetry breaking time for the different treatments.

Axis and polarity are maintained and the regeneration continues accordingly after healing.

RD model driven via stress-sensitive functions

We base our modeling approach on an established RD mechanism that was previously used to describe the regeneration of *Hydra* head organizers and was originally studied in this context by Gierer and Meinhardt (24). Our model extends this work by taking into account the effect of mechanical transformations on the diffusion processes in the *Hydra* cell layer. The two main properties of the extension are that 1), strong mechanical oscillations, such as the inflation-collapse cycles observed experimentally, are required to attain morphogen gradients; and 2), the transformation of *Hydra*'s shape at symmetry breaking is linked to the formation of stable gradients (Fig. 6 *A*).

Based on work by Meinhardt and co-workers, we model the *Hydra* cell ball by a continuous system, which is justified

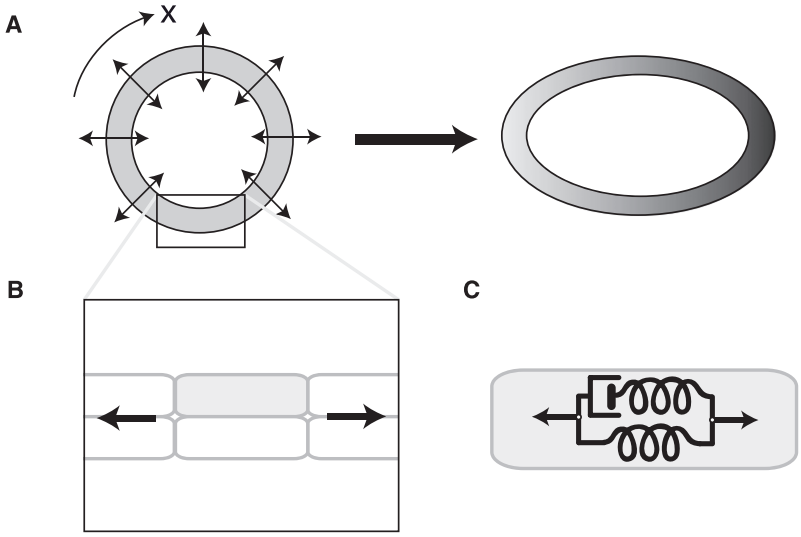

FIGURE 6 (*A*) The model for *Hydra* symmetry breaking consists of a reaction-diffusion equation given on a periodic domain of length L. The domain with coordinate x corresponds to the circumference of the *Hydra* cell ball. The mechanical oscillations together with the Turing instability break the initial isotropy of the system. This triggers further biochemical steps that permanently transform the sphere into an elongated ellipsoid, displaying a nonhomogenous distribution of activator and inhibitor due to the reaction-diffusion instability. (*B*) The role of oscillations in our model is to create a periodic tangential extension of the cell layers, which in turn modifies the transport rate of morphogens. (*C*) Cells have viscoelastic properties that can be modeled by combinations of viscous dash-pots and elastic springs. The shear moduli depend on the frequency of oscillatory deformations for small frequencies.

for our purposes owing to the large number of cells (~10^4) on a typical *Hydra* sphere. The generalized diffusion of morphogens in the tissue is assumed to include diffusion in the extracellular space, as well as transport in the cells. The latter can be direct transport or indirect transport by signaling processes. All of these processes can be described by effective diffusion mechanisms (39–41).

The simplest reaction-diffusion model for *Hydra* consists of two species—an activator, c, and an inhibitor, h—and possesses two diffusion coefficients, σ and μ, for the activator and inhibitor, respectively. These components, together with appropriate kinetics of the two substances, are sufficient for a pattern-forming instability named after Turing (20). A crucial point is that the Turing mechanism requires that the diffusion coefficient for the activator be much smaller than that of the inhibitor, i.e., $\sigma \ll \mu$. Koch and Meinhardt introduced the following minimum model equations (42):

$$\partial_t c = \rho_c\left(c^2/h - c\right) + \sigma\partial_x^2 c, \tag{1}$$

$$\partial_t h = \rho_h\left(c^2 - h\right) + \mu\partial_x^2 h. \tag{2}$$

Here, ρ_c and ρ_h are the production and removal rates. It is essential for our model that the system forms patterns only if the diffusion contrast is strong enough, i.e., if the parameter σ becomes small compared to μ. Mathematically, the pattern grows from the trivial homogenous state through a linear instability if the parameter μ is larger than a critical μ_c, provided that all other parameters remain constant. Relating this fact to the *Hydra* cell ball, we identify the nonoscillating, homogeneous tissue with the regime $\mu < \mu_c$, whereas the oscillating developing cell ball corresponds to a μ that is, at least on average, $>\mu_c$.

We therefore propose that deformations during the inflation-collapse oscillations of the cell ball cause tangential stretching of cells during the swelling phase (Fig. 6 *B*), and that the corresponding stress in turn leads to changes in the transport of signaling molecules, such as the activator or inhibitor. The mobility of molecules could be modulated, for instance, by stress-sensitive channels that are known to open or close when tension is exerted by the membrane or the cytoskeleton (43), or when the cytoskeletal structure changes in response to stress.

According to this argument, the inflation-collapse cycles lead to a periodic modulation of diffusion coefficients. For simplicity, we will assume here that the stretching of cells causes an increase in inhibitor transport, whereas the activator transport remains unaffected. The argument works equally well with a reduction of activator mobility and unchanged inhibitor mobility. More generally, the mathematical mechanism can be applied to any parameter of the model that is mechanodependent and driven into the Turing unstable range due to the oscillations.

An important observation from the experiments is that since regeneration is observed only if the cell ball undergoes inflation-collapse cycles, the system must be driven into the Turing unstable regime during the swelling phase at each cycle. In other words, the cells are 1), in a stable regime before each inflation, 2), in the Turing unstable regime after the inflation has passed a certain threshold, and 3), in the stable regime after the collapse. Only if the inflation stage is sufficiently long or sufficiently intense will the net result be a pattern instability (see Fig. 7).

As stated above, we will assume that the mechanical deformations affect only the inhibitor. Based on Fig. 7 *B*, we can then make a sawtooth ansatz for the evolution of the inhibitor diffusion coefficient:

$$\mu = \mu_0 + 2\Delta\mu\left(t \bmod \frac{1}{\omega}\right), \tag{3}$$

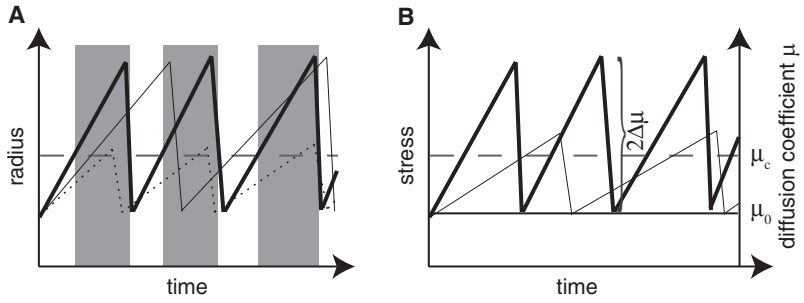

FIGURE 7 Schematic representation of the evolution of radius, stress, and diffusion coefficient during phase I oscillations. (*A*) The system becomes unstable when a certain threshold (*horizontal dashed line*) is exceeded. Strong oscillations (*solid black lines*) drive the system into the unstable regime (*gray areas*). If the oscillations are too weak (*dotted line*), the system does not remain in the unstable region for sufficient time to develop the instability. (*B*) Corresponding evolution of the stress during the pulses. Microrheological studies (33) showed a power law dependence of shear moduli with frequency. Hence, the differential stress is smaller for slow oscillations (*thin black lines* in *A* and *B*) than for fast oscillations (*thick black lines*) if the differential radius is equal. Since we assume a linear relation between inhibitor transport and stress, the plots also represent the modulation of diffusion coefficient μ. μ_c is the critical diffusion coefficient above which Eqs. 1 and 2 are in the Turing unstable regime.

where ω represents the frequency of cycles and $2\Delta\mu$ is the amplitude of the modulation. $t \bmod T = t - nT$ if $nT < t < (n + 1)T$ (where n is an integer number) and is used to describe the sawtoothlike evolution in time t.

In view of the argument given above, the system is in the stable regime as long as $\mu = \mu_0$ ($\Delta\mu = 0$, see Fig. 7). Our model then possesses the property that oscillations for which $\Delta\mu > \mu_c$ drive the system into the Turing unstable regime and therefore generate the force to amplify small fluctuations toward the growth of a nonhomogenous pattern.

Last, we describe how the diffusivity variation, $\Delta\mu$, depends on the parameters of the mechanical oscillations (i.e., the amplitude of oscillations defined from the radius, $A = \langle r_{\max} - r_{\min} \rangle$, and the frequency, ω). An essential point of our model is that cells are viscoelastic objects (Fig. 6 *C*) (44,45). The *Hydra* cells are subjected to an oscillating stress during the swelling cycles. Because the stress, and not the strain, describes the transient response to a mechanical perturbation, we will here take this oscillating stress, instead of the variation in radius, to be the quantity that modulates the diffusion coefficient in Eq. 3. Therefore, we need a relation between stress variation and the parameters A and ω.

For oscillatory mechanical deformations, the stress variation depends on the frequency of periodic deformations in a complex way. As described in Hoffman et al. (33), the shear moduli scale with frequency with an exponent γ close to 0.3. Since the amplitude of stress variation should follow the same scaling, we complete our model by identifying $\Delta\mu$ in Eq. 3 at first, linear order with the amplitude of stress modulation:

$$\Delta\mu = \alpha\omega^{\gamma}, \tag{4}$$

where α is proportional to the amplitude, A, of oscillations. Qualitatively, this effect results in a smaller amplitude, $\Delta\mu$, of oscillations of the inhibitor diffusivity for slow deformations (Fig. 7). In the limit of very slow deformations, no stress is generated, and consequently, stress-sensitive cellular functions are not activated.

Fig. 4 contains a fit of the symmetry breaking time from experimental data to a form $a/[(b\omega)^{\gamma} - 1]$. This fitting is expected on general grounds if a system is close to a linear instability, as follows. Using a time-averaged Eq. 3 to approximate $\mu = \mu_0 + \Delta\mu$, the growth rate, λ, of a small perturbation in the system depends on μ as $\lambda = \lambda(\mu_0) + b'\Delta\mu + O(\Delta\mu^2)$. Note that we assume that the system is linearly stable if $\Delta\mu = 0$, i.e., $\lambda(\mu_0) < 0$. Then, with Eq. 4, we can approximate to linear order

$$\lambda = \lambda(\mu_0) + b' \alpha\omega^{\gamma}. \tag{5}$$

After rescaling $a = -1/\lambda(\mu_0)$ and $b = [-b'\alpha/\lambda(\mu_0)]^{(1/\gamma)}$ and taking the inverse of λ, we find for the symmetry breaking time

$$t_{\mathrm{SB}} \sim \frac{1}{\lambda} = \frac{a}{(b\omega)^{\gamma} - 1}. \tag{6}$$

This fitting function with $\gamma = 0.3$ was used for the experimental data (Fig. 4).

A further observation that supports the reaction-diffusion argument is that the experimental t_{SB} fits a parabolic dependence on the cell ball's initial size (Fig. 2). In the reaction-diffusion model, the initial size corresponds to the length of a periodic domain on which the equations are solved. As described above, we identify the position coordinate in the periodic domain with the coordinate along the circumference of the cell ball. The rate at which a small perturbation of the initially homogeneous pattern grows in the reaction-diffusion model can be calculated under the assumption that the system is close to the Turing instability. In general, the growth rate λ is then given by $\lambda = \lambda_0 - \lambda_1(2\pi/L - k_c)^2$, where k_c is the Turing critical wave number and L is the length of the periodic domain. It can then be shown that the time for the growth of the perturbation is proportional to $1/\lambda = 1/\lambda_0 + \mathrm{const}(L - 2\pi/k_c)^2$. This parabolic form clearly explains the optimal size for symmetry breaking observed experimentally (see Fig. 2).

Note that we here consider the case of a system with one head organizer only. In a reaction-diffusion description, this case corresponds to a domain size close to the critical wavelength. On the other hand, for systems that fit exactly two or more of the critical wavelengths (e.g., large aggregates), one would expect a symmetry breaking time for each domain that is similar to the case of one head organizer. The increase of

t_{SB} discussed in the previous paragraph is therefore a result of a finite size close to the critical wavelength.

We have also tested the predictions of our model for the dependence of t_{SB} on the amplitude A of cycles, i.e., the difference in sphere radius from the beginning of a cycle to the end. In the experiments, the full amplitude of inflation fluctuates by ~30% for a number of *Hydra* balls with similar initial size. In the model, this fluctuation corresponds to a change of α (proportional to A) and, based on the argument used for ω, t_{SB} should depend on the amplitude α. In experiments, this effect could not be identified. We believe that the fluctuations of 30% are simply too small to have a detectable effect compared to the much stronger variations in ω.

DISCUSSION

We have studied the relation between morphogenetic processes and mechanical properties of the regenerating *Hydra* cell ball. Changes at the molecular level lead to the emergence of a head organizer (a weak spot in the *Hydra* ball), which modifies the elastic properties of the tissue and the trait of the mechanical oscillations. It came as a surprise that the mechanical oscillations also influence the morphogenetic processes. There is clear evidence of this in our observation that the time for pattern development, as identified by the symmetry breaking time, strongly depends on the frequency of oscillations. The frequency of oscillations can be externally controlled by the osmolarity of the *Hydra* medium.

A Turing mechanism driven by mechanical oscillations (in the form of the inflation-collapse cycles observed experimentally) provides the minimal components to describe symmetry breaking and the formation of the organizer. Our model is based on the idea that the diffusion coefficients of the activator and inhibitor change during the swelling stages of the *Hydra* ball. The fundamental condition for Turing instability—a strong difference in diffusivities—is established once a critical mechanical stress is reached. A pattern (the organizer) is generated that identifies the morphogenetic symmetry breaking moment.

Although we are indeed interested in the morphogenetic time, we can currently measure it only indirectly as the mechanical symmetry breaking time, which is given experimentally by the transition from phase I to phase II oscillations. However, it is possible that by this indirect measurement the morphogenetic symmetry breaking time is overestimated. Hobmayer et al. (4), for instance, found evidence that one of the early signaling molecules involved in a possible reaction-diffusion process is β-catenin. Head organizer factors such as Wnt (and therefore the mouth opening itself) appear later, thus contributing to a possible delay between patterning and mechanical changes. Since recent studies have pointed out an interrelation between β-catenin and Wnt pathways (46), we infer that the delay between the two processes is probably short. Indeed, by comparing our results with the experiments of Hobmayer et al. (4) on Wnt expression during head regeneration, we estimate this delay to be ~2 h. This time is on the order of an inflation-collapse cycle and therefore below the temporal resolution of our experiments.

There is evidence, described in recent reports, that cells indeed can sense forces and geometry not only for mechanical adaptation but also for control of gene expression (27,28). For instance, transcription factors could associate to force-sensitive adhesion sites or be modified in a force-dependent way before carrying the signal to the nucleus (47). It is also known that the action of some ion channels, as well as the cytoskeletal structure, depends on mechanical forces, which may further influence the transport of a morphogenetic signal.

To simplify the model, we here consider only the effect of stretch on transport of a signaling substance. We build on the fundamental role of differential diffusion rates for Turing patterning and postulate that the inflation-collapse cycles modulate the morphogen transport, thus providing the critical driving force for symmetry breaking. The rate of diffusion is therefore changed depending on the mechanical stress (e.g., through mechanosensitive channels) and oscillates periodically with the *Hydra* cell ball. Our relation between diffusion rate and stress couples mechanical and biochemical parameters at first, linear order.

We have observed experimentally that the symmetry breaking time, t_{SB}, depends strongly on the frequency of the oscillations, f. To reflect this behavior, we have included in the model the further ingredient that the shear moduli (and therefore the stress variation) depend on the frequency if cells are deformed in an oscillatory manner.

From the mechanically coupled RD equations we then predict that t_{SB} decreases with the swelling rate and frequency of the oscillations with a behavior that is given by a function of the form $t_{SB} = a/[(bf)^{\gamma} - 1]$. We have found that this relation describes the experimental results strikingly well.

Our model also provides an explanation for the presence of an optimum size, i.e., that spheres with radii of $\simeq 140\ \mu$m regenerate faster. This result is a very general consequence for a reaction-diffusion model and thus also provides a strong additional support for the use of reaction-diffusion mechanisms for *Hydra* regeneration.

However, our model does not address the question of what happens after the formation of the organizer. Once the gradient is spontaneously established in the *Hydra* due to the Turing instability, the large-amplitude oscillations are suppressed. Consequently, in the framework of a reaction-diffusion model, an additional mechanism is needed to explain the sustained differential diffusion properties. The experimental observation that important changes at the cellular level take place after symmetry breaking suggests that the presence of the pattern induces irreversible cell differentiation that locks the axis and therefore maintains

Hydra activator/inhibitor gradient. In this sense, the phase I oscillations are not further required.

According to our model, the patterning process only takes place in an oscillating cell ball. Therefore, we suggest the following biological purpose of the oscillations. The *Hydra* cell ball has to be closed for an osmotic pressure to build up and the cell ball to oscillate, and only under this condition should regeneration be started. This provides a mechanism for global cell communication and sensing, since the cells will be under mechanical stress only if others are present and if the topology is closed. Such a mechanism could be crucial during the formation of the first multicellular organisms.

In summary, we have shown that a reaction-diffusion mechanism provides a suitable scenario to describe *Hydra* symmetry breaking during regeneration from a cell ball. We introduced a model in which the swelling of the initial *Hydra* cell ball induces changes in the diffusivity rates of activator and inhibitor. The mechanical stress provided by the oscillations drives the system to the unstable regime. Once the organizer is constituted and a chemical gradient established, the organizer locks and maintains the axis, and the oscillations are no longer required. Analytical considerations of the model show that the symmetry breaking time decreases with the swelling rate with the same behavior observed experimentally.

Our experimental results provide strong evidence that morphogenic oscillations play a pivotal role during axis definition in *Hydra* development. Assuming a coupling of cell signaling and mechanical cell stress, which seems difficult to imagine otherwise, the experimental observations agree well with a Turing instability. This coupling enables a symmetry breaking mechanism as a natural extension of the well established reaction-diffusion picture.

We are very grateful to T. C. G. Bosch at the University of Kiel (Kiel, Germany) for fruitful discussions, encouragement, and technical assistance. We also thank A. Hanold (University of Bayreuth, Bayreuth, Germany) for continuous technical assistance.

This research was supported by the European Training Network PHYNECS of the European Commission, under project HPRN-CT-2002-00312. J.S. also acknowledges the support of the Minerva Foundation (Munich, Germany) and the Curwen-Lowy Fellowship.

REFERENCES

1. Riechmann, V., and A. Ephrussi. 2001. Axis formation during *Drosophila* oogenesis. *Curr. Opin. Genet. Dev.* 11:374–383.
2. Wolpert, L., J. Smith, T. Jessell, P. Lawrence, E. Robertson, et al. 2006. Principles of Development, 3rd ed. Oxford University Press, Oxford.
3. Fowler, J., and R. Quatrano. 1995. Cell polarity, asymmetric division, and cell fate determination in brown algal zygotes. *Semin. Dev. Biol.* 6:347–358.
4. Hobmayer, B., F. Rentzsch, K. Kuhn, C. M. Happel, C. C. von Laue, et al. 2000. Wnt signalling molecules act in axis formation in the diploblastic metazoan Hydra. *Nature*. 407:186–189.
5. Broun, M., and H. R. Bode. 2002. Characterization of the head organizer in *Hydra*. *Development*. 129:875–884.
6. Broun, M., L. Gee, B. Reinhardt, and H. R. Bode. 2005. Formation of the head organizer in *Hydra* involves the canonical Wnt pathway. *Development*. 132:2907–2916.
7. Bode, H. R. 2003. Head regeneration in *Hydra*. *Dev. Dyn.* 226:225–236.
8. MacWilliams, H. K. 1983. Hydra transplantation phenomena and the mechanism of *Hydra* head regeneration. II. Properties of the head inhibition. *Dev. Biol.* 96:217–238.
9. MacWilliams, H. 1983. Hydra transplantation phenomena and the mechanism of *Hydra* head regeneration. Properties of the head activation. *Dev. Biol.* 96:239–257.
10. Bosch, T. 2007. Why polyps regenerate and we don't: towards a cellular and molecular framework for *Hydra* regeneration. *Dev. Biol.* 303:421–433.
11. Sánchez, A. 2000. Regeneration in the metazoans: why does it happen? Bioessays. 22:578–590.
12. Holstein, T., E. Hobmayer, and U. Technau. 2003. Cnidarians: an evolutionarily conserved model system for regeneration? Dev. Dyn. 226:257–267.
13. Gierer, A., S. Berking, H. Bode, C. David, K. Flick, et al. 1972. Regeneration of *Hydra* from reaggregated cells. *Nat. New Biol.* 239:98–101.
14. Shimizu, H., Y. Sawada, and T. Sugiyama. 1993. Minimum tissue size required for *Hydra* regeneration. *Dev. Biol.* 155:287–296.
15. Technau, U., C. C. von Laue, F. Rentzsch, S. Luft, B. Hobmayer, et al. 2000. Parameters of self-organization in *Hydra* aggregates. *Proc. Natl. Acad. Sci. USA*. 97:12127–12131.
16. Fütterer, C., C. Colombo, F. Jülicher, and A. Ott. 2003. Morphogenetic oscillations during symmetry breaking of regenerating *Hydra* vulgaris cells. *Europhys. Lett.* 64:137–143.
17. Soriano, J., C. Colombo, and A. Ott. 2006. Hydra molecular network teaches vriticality at the dymmetry-breaking axis-defining moment. *Phys. Rev. Lett.* 97:258102.
18. Beloussov, L., N. Kazakova, N. Luchinskaia, and V. Novoselov. 1997. Studies in developmental cytomechanic. *Int. J. Dev. Biol.* 41:793–799.
19. Kücken, M., J. Soriano, P. Pullarkat, A. Ott, and E. M. Nicola. 2008. An osmoregulatory basis for volume oscillations in regenerating *Hydra*. *Biophys. J.* 95:978–985.
20. Turing, A. M. 1952. The chemical basis of morphogenesis. *Philos. Trans. R. Soc. Lond. B Biol. Sci.* 237:37–72.
21. Murray, J. D. 2005. Mathematical Biology, 3rd ed. Springer, Berlin.
22. Summerbell, D. 1983. The effect of local application of retinoic acid to the anterior margin of the developing chick limb. *J. Embryol. Exp. Morphol.* 78:269–289.
23. Harris, M. P., S. Williamson, J. F. Fallon, H. Meinhardt, and R. O. Prum. 2005. Molecular evidence for an activator-inhibitor mechanism in the development of embryonic feather branching. *Proc. Natl. Acad. Sci. USA*. 102:11734–11739.
24. Gierer, A., and H. Meinhardt. 1972. A theory of biological pattern formation. *Kybernetik*. 12:30–39.
25. Meinhardt, H., and A. Gierer. 2000. Pattern formation by local self-activation and lateral inhibition. *Bioessays*. 22:753–760.
26. Meinhardt, H. 2007. Models of biological pattern formation: from elementary steps to the organization of embryonic axes. *Curr. Top. Dev. Biol.* 81:1–63.
27. Brouzes, E., W. Supatto, and E. Farge. 2004. Is mechano-sensitive expression of twist involved in mesoderm formation? Biol. Cell. 96:471–477.
28. Brouzes, E., and E. Farge. 2004. Interplay of mechanical deformation and patterned gene expression in developing embryos. *Curr. Opin. Genet. Dev.* 14:367–374.
29. Dike, L. E., C. S. Chen, M. Mrksich, J. Tien, G. M. Whitesides, et al. 1999. Geometric control of switching between growth, apoptosis, and differentiation during angiogenesis using micropatterned substrates. *In Vitro Cell. Dev. Biol. Anim.* 35:441–448.
30. Cardenas, M., Y. Fabila, S. Yum, J. Cerbon, F. D. Bohmer, et al. 2000. Selective protein kinase inhibitors block head-specific differentiation in *Hydra*. *Cell. Signal.* 12:649–658.

31. Kishimoto, Y., M. Murate, and T. Sugiyama. 1996. Hydra regeneration from recombined ectodermal and endodermal tissue. I. Epibolic ectodermal spreading is driven by cell intercalation. J. *Cell Sci.* 109:763–772.

32. Lily, S. J. 1956. Osmoregulation and ionic regulation in *Hydra*. *J. Exp. Biol.* 32:423–439.

33. Hoffman, B., G. Massiera, K. V. Citters, and J. Crocker. 2006. The consensus mechanics of cultured mammalian cells. *Proc. Natl. Acad. Sci. USA.* 103:10259–10264.

34. Fei, K., L. Yan, J. Zhang, and M. P. Sarras, Jr.. 2000. Molecular and biological characterization of a zonula occlundens-1 homologue in *Hydra vulgaris*, named HZO-1. *Dev. Genes Evol.* 210:611–616.

35. Amit, S., A. Hatzubai, Y. Birman, J. Andersen, E. Ben-Shushan, et al. 2002. Axin-mediated CKI phosphorylation of β-catenin at Ser 45: a molecular switch for the Wnt pathway. *Genes Dev.* 16:1066–1076.

36. Kaloulis, K., S. Chera, M. Hassel, D. Gauchat, and B. Galliot. 2004. Reactivation of developmental programs: the cAMP-response element-binding protein pathway is involved in *Hydra* head regeneration. *Proc. Natl. Acad. Sci. USA.* 101:2363–2368.

37. Tamaoki, T., H. Nomoto, I. Takahashi, Y. Kato, M. Morimoto, et al. 1986. Staurosporine, a potent inhibitor of phospholipid/Ca^{++}-dependent protein kinase. *Biochem. Biophys. Res. Commun.* 135:397–402.

38. Reference deleted in proof.

39. Roussel, C. J., and M. R. Roussel. 2004. Reaction-diffusion models of development with state-dependent diffusion coefficients. *Prog. Biophys. Mol. Biol.* 86:113–160.

40. Keener, J. and J. Sneyd. Mathematical Physiology: II: Systems Physiology. Springer, 2008.

41. Bollenbach, T., K. Kruse, P. Pantazis, M. Gonzalez-Gaitan, and F. Jülicher. 2005. Robust formation of morphogen gradients. *Phys. Rev. Lett.* 94:018103.

42. Koch, A. J., and H. Meinhardt. 1994. Biological pattern formation: from basic mechanisms to complex structures. *Rev. Mod. Phys.* 66:1481–1507.

43. Wehner, F., H. Olsen, H. Tinel, E. Kinne-Saffran, and R. Kinne. 2003. Cell volume regulation: osmolytes, osmolyte transport, and signal transduction. *Rev. Physiol. Biochem. Pharmacol.* 148:1–80.

44. Pullarkat, P. A., P. A. Fernández, and A. Ott. 2007. Rheological properties of the eukaryotic cell cytoskeleton. *Phys. Rep.* 449:29–53.

45. Fernández, P. A., L. Heymann, A. Ott, N. Aksel, and P. A. Pullarkat. 2007. Shear rheology of a cell monolayer. *New J. Phys.* 9:419.

46. Nelson, W., and R. Nusse. 2004. Convergence of Wnt, β-catenin, and cadherin pathways. *Science.* 303:1483–1487.

47. Vogel, V., and M. Sheetz. 2006. Local force and geometry sensing regulate cell functions. *Nat. Rev. Mol. Cell Biol.* 7:265–275.